EKF/UKF Maneuvering Target Tracking using Coordinated Turn Models with Polar/Cartesian Velocity

Conference Paper · July 2014

CITATIONS
88

READS
2,069

3 authors, including:

Michael Roth
German Aerospace Center (DLR)
48 PUBLICATIONS **848** CITATIONS
SEE PROFILE

Gustaf Hendeby
Linköping University
183 PUBLICATIONS **2,666** CITATIONS
SEE PROFILE

EKF/UKF Maneuvering Target Tracking using Coordinated Turn Models with Polar/Cartesian Velocity

Michael Roth*, Gustaf Hendeby*†, and Fredrik Gustafsson*
*Dept. Electrical Engineering, Linköping University, SE-581 83 Linköping, Sweden.
Email: {roth, hendeby, fredrik}@isy.liu.se
†Dept. of Sensor & EW Systems, Swedish Defence Research Agency (FOI), SE-581 11, Linköping, Sweden.
Email: gustaf.hendeby@foi.se

***Abstract*—Nonlinear Kalman filter adaptations such as extended Kalman filters (EKF) or unscented Kalman filters (UKF) provide approximate solutions to state estimation problems in nonlinear models. The algorithms utilize mean values and covariance matrices to represent the probability densities in the otherwise intractable Bayesian filtering equations. As a consequence, their estimation performance can show significant dependence on the choice of state coordinates. The here considered problem of tracking maneuvering targets using coordinated turn (CT) models is one practically relevant example: The velocity in the target state can either be formulated in Cartesian or polar coordinates. We extend a previous study to a broader range of CT models that allow for changes in target speed and turn rate, and investigate UKF as well as EKF variants in terms of their performance and sensitivity to noise parameters. The results advocate for the use of polar CT models.**

I. Introduction

We investigate tracking of maneuvering targets under the assumption of *coordinated turn* (CT) target motion. The CT models that we consider describe horizontal motion at nearly constant speed along circle segments, as commonly encountered in aviation, and appear in different flavors throughout the tracking and filtering literature [1–5]. Kalman filter variants that are based on these models are important building blocks of *interacting multiple model* (IMM) filters [2].

Within the IMM framework, Kalman filters with CT models are typically used to track the target during maneuvers [3, 6]. Our investigation concentrates on nonlinear CT variants that allow for varying turn rate as well as varying target speed, in contrast to their linear cousins with known turn rate [5]. This choice is backed by an analysis of real world aircraft data [7] that advocates for the varying speed and turn rate assumption. A potential benefit [3] of an IMM algorithm with these more flexible CT models is a reduced number of required modes.

The nonlinear nature of the considered CT models requires the use of nonlinear Kalman filter adaptations such as *extended Kalman filters* [8] (EKF) or *unscented Kalman filters* [9] (UKF). One consequence of the inherent approximations in such algorithms is that the estimation performance depends on the choice of the state coordinates. This observation dates back to the early days of Kalman filtering [8] and plays a significant role in target tracking applications [1] where it can alleviate observability issues [10].

We build our work upon the previous study [11] and show how the choice of state coordinates and CT model variants influences the tracking performance for target motion in the horizontal plane. In particular, we compare states that comprise either polar or Cartesian velocity. It is shown how different assumptions on the process noise input during discretization of the underlying CT differential equations yield further model variants for each velocity parametrization and how these can be used for filtering.

In terms of algorithms, we investigate the UKF as well as the EKF variants that were covered in [11]. We provide performance results for a range of CT Kalman filters and analyze their sensitivity with respect to the noise parameters of the stochastic CT models. This is done via *Monte Carlo* (MC) simulations on a set of benchmark trajectories taken from [12], with emphasis on segments that correspond to target maneuvers. All filters are operated with range and bearing measurements that are transformed to Cartesian positions and use individually optimized process noise parameters so as to facilitate a fair comparison of the model and filter choice.

The outline of the paper is as follows. The employed CT models are introduced in Section II. Kalman filter adaptations for nonlinear estimation problems are described in Section III. The conducted experiment and a discussion of obtained results are given in Section IV. Conclusions are given in Section V.

II. Coordinated Turn Models

The list of available motion models used for tracking is long. Extensive sources include the survey [5] or the dedicated chapters in [4]. In this section we describe the underlying continuous-time dynamics before deriving discrete time models based on polar and Cartesian velocity representations. Finally, we discuss the noise inputs of stochastic CT models.

A. From Particle Motion to Discrete-time CT Models

Our focus is on coordinated turn models which have their origin in curvilinear particle motion [5]. Figure 1 illustrates the involved variables. The target position in the horizontal plane

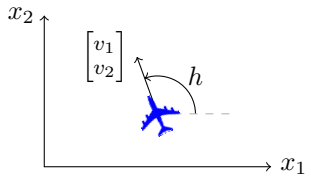

Fig. 1. Illustration of state components. The target is depicted in the x_1–x_2–plane. The attached velocity vector has components v_1 and v_2 in x_1 and x_2 direction, respectively. v is the magnitude of the velocity vector and h the heading angle.

with respect to a fixed Cartesian coordinate frame is denoted by x_1 and x_2 [m]; the velocity vector has components v_1 and v_2 and magnitude v, all [m/s]; h [rad] denotes the heading angle, given by the two argument arctangent $\mathrm{atan2}(v_2, v_1)$. Furthermore, we define the turn rate $\omega = \frac{dh}{dt}$ [rad/s] as the time derivative of the heading angle.

We assume that the target is driven by linear and rotational acceleration inputs a [m/s^2] and α [rad/s^2], respectively. Here, a is also known as longitudinal acceleration that acts tangential to the target path, thus aligned with the Cartesian velocity vector. While a accounts for speed changes, α influences the turn rate. The coupled differential equations

$$\begin{bmatrix} \dot{x}_1 \\ \dot{x}_2 \\ \dot{v} \\ \dot{h} \\ \dot{\omega} \end{bmatrix} = \begin{bmatrix} v\cos(h) \\ v\sin(h) \\ a \\ \omega \\ \alpha \end{bmatrix} \tag{1}$$

form a continuous-time state equation for the target state $x = \begin{bmatrix} x_1 & x_2 & v & h & \omega \end{bmatrix}^{\mathrm{T}}$ with velocity in polar coordinates. The position entries in (1) depend nonlinearly on h, whereas the acceleration inputs a and α enter linearly.

If we change to a state with Cartesian velocity, $x = \begin{bmatrix} x_1 & x_2 & v_1 & v_2 & \omega \end{bmatrix}^{\mathrm{T}}$, the resulting differential equation

$$\begin{bmatrix} \dot{x}_1 \\ \dot{x}_2 \\ \dot{v}_1 \\ \dot{v}_2 \\ \dot{\omega} \end{bmatrix} = \begin{bmatrix} v_1 \\ v_2 \\ a\cos(h) - v_2\omega \\ a\sin(h) + v_1\omega \\ \alpha \end{bmatrix} \tag{2}$$

exhibits bilinear relations $v_1\omega$ and $v_2\omega$. Furthermore, the assumption of mere longitudinal acceleration (apart from the turning acceleration) now yields a nonlinear dependency on $h = \mathrm{atan2}(v_2, v_1)$ in the velocity. The coordinate change relating the two state vectors is obvious from the first two components in (1) and (2).

The state differential equations (1) and (2) are both in the form $\dot{x} = \varphi(x, a, \alpha)$. Hence, we need to first discretize in order to apply discrete-time filtering techniques later. This amounts to (approximately) solving (1) and (2) for the state at time instance $k+1$ given the state at time k, an initial value problem. The results we obtain turn out to be of the form

$$x_{k+1} = f(x_k) + G(x_k)w_k, \tag{3}$$

where the indices denote sampling instants and $w = \begin{bmatrix} a & \alpha \end{bmatrix}^{\mathrm{T}}$ comprises the acceleration inputs. The sample time T enters the expression implicitly. For simplicity we treat w as deterministic and introduce randomness once the discrete-time equations have been established. Schemes that discretize related models under the assumption of random inputs are shown in [13] and [14], where the latter considers ω not as part of the state but as input.

B. Coordinated Turn with Polar Velocity

We begin with the discretization of (1) which is in general not trivial. For $a = 0$ and $\alpha = 0$, however, a compact solution to the differential equations is readily available and given by

$$f_p(x) = \begin{bmatrix} x_1 + \frac{2v}{\omega}\sin(\frac{\omega T}{2})\cos(h + \frac{\omega T}{2}) \\ x_2 + \frac{2v}{\omega}\sin(\frac{\omega T}{2})\sin(h + \frac{\omega T}{2}) \\ v \\ h + \omega T \\ \omega \end{bmatrix}. \tag{4}$$

The index p stands for "polar" and, naturally, $f_p(x)$ takes states with polar velocity as input argument. Equation (4) is given in [11] but equivalent solutions can also be found elsewhere [15].

If we assume non-zero a and α, the solutions to (1) become increasingly complicated, depending on the behavior of a and α between sampling instants. A discussion of such discretization problems, including suggested solutions, is provided in [4]. Here, we settle for using (4) and concentrate on the input part of (3), which amounts to finding $G(x)$. We investigate two schemes of which the first asserts that a and α act as impulses just before each sampling instant. Consequently, each input acts only on the state components that are directly influenced. The second approach assumes that a and α are constant between sampling instants, and is commonly known as zero-order-hold discretization. For the linear part (v, h, ω) of (1) the solution for constant w is easily derived, but the solution for (x_1, x_2) becomes very complicated due to the time-varying h. Euler's method, *i.e.*, asserting a constant h between sampling instants, yields a simple approximate solution. The resulting $G(x)$ of (3) are given by

$$G_p^1 = \begin{bmatrix} 0 & 0 \\ 0 & 0 \\ T & 0 \\ 0 & 0 \\ 0 & T \end{bmatrix}, \qquad G_p^2(h) = \begin{bmatrix} \frac{T^2}{2}\cos(h) & 0 \\ \frac{T^2}{2}\sin(h) & \\ T & 0 \\ 0 & \frac{T^2}{2} \\ 0 & T \end{bmatrix} \tag{5}$$

for the impulse and constant interpretations of w, respectively. Obviously, G_p^1 is independent of the state.

C. Coordinated Turn with Cartesian Velocity

The discrete-time version of (2) follows from (4) by converting from polar to Cartesian velocity and is given by

$$f_c(x) = \begin{bmatrix} x_1 + \frac{v_1}{\omega}\sin(\omega T) - \frac{v_2}{\omega}\big(1-\cos(\omega T)\big) \\ x_2 + \frac{v_1}{\omega}\big(1-\cos(\omega T)\big) + \frac{v_2}{\omega}\sin(\omega T) \\ v_1\cos(\omega T) - v_2\sin(\omega T) \\ v_1\sin(\omega T) + v_2\cos(\omega T) \\ \omega \end{bmatrix}. \quad (6)$$

Solving (2) under the assumption $a = 0$ and $\alpha = 0$ yields equivalent results. Often, (6) is written as product of an ω-dependent matrix with the Cartesian state vector which discloses a linear model for known ω [2, 5]. The corresponding input matrices in (3) follow from arguments similar to those in the polar case and are given by

$$G_c^1(h) = \begin{bmatrix} 0 & 0 \\ 0 & 0 \\ T\cos(h) & 0 \\ T\sin(h) & 0 \\ 0 & T \end{bmatrix}, \quad G_c^2(h) = \begin{bmatrix} \frac{T^2}{2}\cos(h) & 0 \\ \frac{T^2}{2}\sin(h) & 0 \\ T\cos(h) & 0 \\ T\sin(h) & 0 \\ 0 & T \end{bmatrix} \quad (7a)$$

with impulse and constant w, respectively. Since we assume only longitudinal acceleration, $G_c^1(h)$ and $G_c^2(h)$ depend on h, which is a function of v_1 and v_2. Therefore, (7a) appears more nonlinear than (5). Alternatively, a third variant with individual Cartesian acceleration inputs a_1 and a_2 can be formulated. With $w = \begin{bmatrix} a_1 & a_2 & \alpha \end{bmatrix}^{\mathrm{T}}$ we obtain

$$G_c^3 = \begin{bmatrix} \frac{T^2}{2} & 0 & 0 \\ 0 & \frac{T^2}{2} & 0 \\ T & 0 & 0 \\ 0 & T & 0 \\ 0 & 0 & T \end{bmatrix}. \quad (7b)$$

Combining (6) and (7b) yields a widespread CT model variant [2, 5]. Obviously, G_c^3 does not depend on the state and the resulting model allows acceleration in any direction, in contrast to the longitudinal only acceleration that we assumed before. In this respect, G_c^3 bears a close resemblance to the input matrix of *constant velocity models* [4, 5].

D. Process Noise Assumptions

So far, we have discussed different *deterministic* CT models that employ polar or Cartesian velocity. In order to obtain a *stochastic* CT model, we formulate a probabilistic description of the input signals a and α. As indicated earlier, we pursue a direct discrete-time approach [2] rather than discretizing random processes, which means that we treat a and α (whether impulse or constant between sampling instants) as uncorrelated random variables with zero mean and standard deviations σ_a [m/s^2] and σ_α [rad/s^2]. Furthermore, we treat the obtained noise sequences a_k and α_k as white. The zero-mean input yields the typical nearly constant speed and nearly constant turn rate behavior that is widely used in motion models for filtering. In fact, some authors prefer the name (nearly) *constant turn models* to make a distinction to the more complex coordinated turns in aviation [5].

III. EKF and UKF for Nonlinear Filtering

In this section, an overview of different Kalman filter variants for nonlinear filtering is provided. For a more extensive treatment of filtering theory and the actual algorithms, the reader is referred to [4] and the references below.

A. Bayesian Filtering Theory

Filtering in nonlinear state-space models is a difficult problem. The widely accepted Bayesian filtering equations [4]

$$p(x_k|y_{1:k}) = \frac{p(y_k|x_k)p(x_k|y_{1:k-1})}{p(y_{1:k})} \quad (8a)$$

$$p(x_k|y_{1:k-1}) = \int p(x_k|x_{k-1})p(x_{k-1}|y_{1:k-1})\,\mathrm{d}x_{k-1} \quad (8b)$$

$$p(y_{1:k}) = \int p(y_k|x_k)p(x_k|y_{1:k-1})\,\mathrm{d}x_k \quad (8c)$$

are conceptually appealing but, due to the required marginalization and conditioning operations, intractable for all but the simplest cases. This has long been known [16]. Hence, considerable effort has been put into the development of algorithms that approximate (8).

The most famous special case for which (8) can be solved comprises a linear state-space model with Gaussian noise and initial state. The solutions are given by a number of recursive update equations that have become known as the *Kalman filter* (KF) [4, 8]. Of course we should note that the KF can be obtained from several different viewpoints that establish further notions of optimality for linear (not necessarily Gaussian) problems [8].

B. Kalman Filter Adaptations for Nonlinear Filtering

It is a natural idea to adapt the Kalman filter to nonlinear problems, and indeed this is where the algorithm made a first considerable impact: The KF was employed to solve nonlinear navigation problems in the Apollo mission [17].

The first nonlinear KF developed became known as the *extended Kalman filter* (EKF), and is based on consecutive linearization of the nonlinear dynamic and measurement equations about current state estimates. The linearization is typically carried out via Taylor series expansion but interpolation schemes based on numerical differentiation also exist [18]. Going beyond linearization, the *second-order EKF* (EKF2) retains the quadratic terms in the Taylor series. This attempt to approximate the system equations more accurately comes at the expense of a vastly increased computational complexity if implemented without further care [19, 20].

A linear approximation cannot fully capture the behavior of a nonlinear system. The *unscented Kalman filter* [9] (UKF) is an algorithm based on *deterministic sampling* that addresses this to some extent. Instead of approximating the state and measurement functions of a nonlinear state space model, few deterministic state realizations — called *sigma points* — are generated and propagated through the involved nonlinearities. The sample statistics of transformed *sigma points* are then used in the KF equations. The main ingredient of the UKF is a computation scheme for transforming mean values and

covariance matrices called *unscented transformation* (UT), which depends on a set of scalar parameters. It turns out that a simple choice of UT parameters yields a *numerical integration rule* of degree 3, and gives rise to a UKF variant called the *cubature Kalman filter* [21] (CKF). The numerical integration viewpoint in the CKF derivation facilitates accuracy statements that are otherwise difficult to obtain for the UKF. A discussion of this can be found in [20]. The fact that UKF variants are sampling based and do not involve Jacobian and Hessian matrices, in contrast to EKF and EKF2, makes them simple to implement.

Relations between UKF and EKF2 have been established in [22]. With the "Gaussian derivation" of the Kalman filter in mind, a common framework for all of the above adaptations can be formulated [20, 22]. After all, KF variants employ the same kind of measurement update equation that is linear in the residual $y_k - \hat{y}_{k|k-1}$, the difference between predicted and measured output. The algorithms differ in the methods that are used for computing mean values and covariance matrices of nonlinearly transformed random variables. An extensive survey of these *moment computation schemes* and their use in Kalman filtering is given in [20].

C. The Role of the State Coordinate System

Kalman filter variants propagate mean values and covariance matrices of filtered and predicted states throughout time. Therefore, a widespread interpretation is that the densities in (8) are assumed to be Gaussian. This is a very restrictive assumption and cannot account for phenomena like multimodality or skewness. As a consequence of the limited flexibility, the choice of state coordinates can have a significant influence on the estimation performance of any nonlinear Kalman filter variant.

IV. Experiment and Discussion

In this section different filter and CT model combinations are assessed on a maneuvering target tracking problem.

A. Experiment Setup

Monte Carlo simulations are used to evaluate the different filters and state-space representations. For this purpose, the six benchmark target trajectories of [12] are used which represent different maneuvering aircraft targets, ranging from a slow cargo aircraft, over smaller maneuverable Learjet-type aircraft, to very agile and fast aircraft. We illustrate the horizontal trajectories in Figure 2 and refer the reader to [12] for a more comprehensive description and further plots, including acceleration magnitude.

The CT models evaluated here cover only two-dimensional CT motion and therefore only the target motion in the horizontal plane is considered. Motivation for such a problem separation is given in [3, 7]. Furthermore, all the trajectories contain considerable constant velocity segments for which the standard KF is known to work very well, whereas CT models are better suited to handle the turns. Several solutions exist to utilize this difference in behavior, the IMM is one. Therefore,

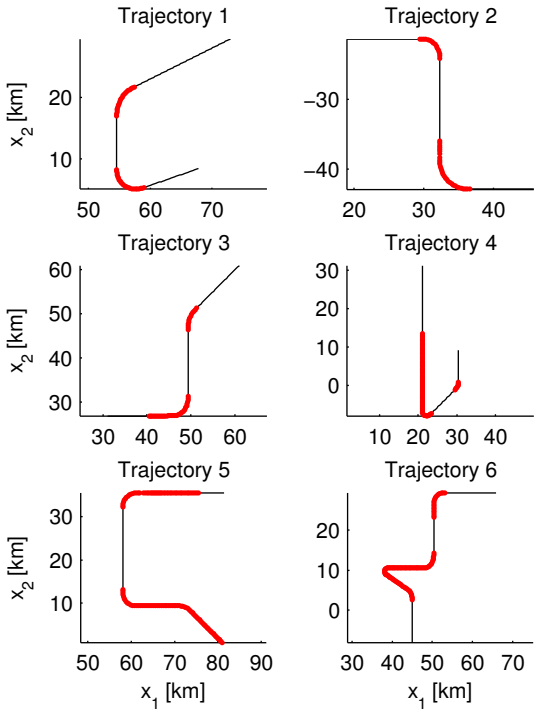

Fig. 2. Trajectories and the segment in which the target is maneuvering (marked in bold red).

to accentuate the behavior during turns, only segments of the trajectories with pronounced acceleration are included in the evaluation. These sections are marked in Figure 2.

For each trajectory, range and bearing measurements are generated by a noisy sensor in the origin, with white Gaussian noise with standard deviation $\sigma_\theta = 0.1$ [°] and $\sigma_r = 100$ [m] for bearing and range, respectively. The measurements and their variances are then converted to Cartesian coordinates to yield position measurements with time-varying measurement covariance matrices. The transformation is performed using both the Gauss approximation and the UT. Both methods produce comparable results for the chosen σ_θ and σ_r.

The tracking performance is evaluated by computing the *root mean square error* (RMSE) for the true target position compared to the predicted state position. We average first over MC realizations and second over time steps. Using the predicted state position instead of the filtered position ensures that we evaluate the full state and the model assumption, not only the position estimate which would be predominant using the filtered position. As mentioned above, only sections of the trajectories with acceleration are included in the RMSE computations. Hence the performance is only evaluated for the highlighted segments in Figure 2.

The specific filters that are compared are EKF, EKF2, and UKF for all CT models of Section II. Per algorithm type this amounts to two polar and three Cartesian models that are tested. For each batch of measurement realizations, the filters are run with different noise settings. Picking the best parameters for all combinations facilitates a fair comparison.

The magnitude of the process noise in each algorithm is varied using a logarithmic scale with a few samples per decade, with the actual measurement noise that was used to generate the measurements. These simulations also indicate how sensitive the filter-model combination is to the process noise parameters. The process noise covariance is computed according to

$$Q_k = G(x_k)\,\mathrm{diag}(\sigma_a^2, \sigma_\alpha^2) G(x_k)^{\mathrm{T}} \tag{9}$$

for all of the filter-model combinations except for those that employ G_c^3 of (7b). There, a slightly altered expression is used.

To set a baseline for the experiments, a linear Kalman filter with *constant velocity* (CV) model is applied along all nonlinear filters. Again, the position RMSE is computed for the several process noise settings so as to find the best possible performance on the maneuver segments of the trajectories.

B. Simulation Results and Discussion

In order to give the reader some qualitative performance insights we illustrate selected results of the best algorithms in each category instead of showing results for all model and filter combinations. We begin by first assessing the linear KF with a CV model, then EKF and UKF with Cartesian CT models, and finally EKF and UKF with polar CT models. The presented RMSE values were computed from the predicted position estimates on 10 measurement realizations.

The UKF variants showed almost no effect to different values of the UT parameters. Therefore, the most basic version of a UKF with zero central weight has been used. This is in fact the CKF of [21].

Figure 3 shows the prediction results that were obtained with the CV KF. Illustrated is the average position RMSE against the logarithm $\log(\sigma_a)$ (base 10) of the acceleration noise standard deviation σ_a that was employed in the KF. The performance on Trajectory 4 is better than on the other trajectories, which can be explained by a longer segment with only minor maneuvering that is well suited to the CV assumption. Furthermore, we include the best RMSE value on each trajectory in the legend. A sensible more advanced algorithm must beat these numbers in order to be worth the extra effort.

Next, we turn to CT models with Cartesian velocity. These require the user to select the two parameters σ_a and σ_α. Figure 4 serves as example for all upcoming illustrations and displays the average position RMSE as contour plot of $\log(\sigma_a)$ and $\log(\sigma_\alpha)$. Dark red areas correspond to parameter choices that produced an RMSE over 200 m. The color scale is valid for the other plots of the same kind. The shown results are for an EKF2 using a CT model with state-dependent input matrix $G_c^2(h)$ of (7a) on Trajectory 1. The best RMSE in the plot title shows that the algorithm clearly outperforms the CV KF. A cross marks the optimal parameter choices.

We begin with an analysis of EKF and compare the three covariance matrices of (7a) and (7b). It turns out that $G_c^2(h)$ of (7a) provides better results than $G_c^1(h)$ and G_c^3. The corresponding RMSE plots are given in Figure 5. Apparently, we can do better than with a CV KF. One exception is

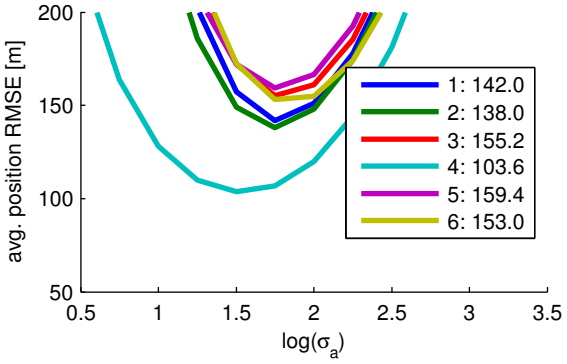

Fig. 3. Average position RMSE [m] of a linear Kalman filter with CV model for all trajectories. Only segments in which the target maneuvers are taken into account.

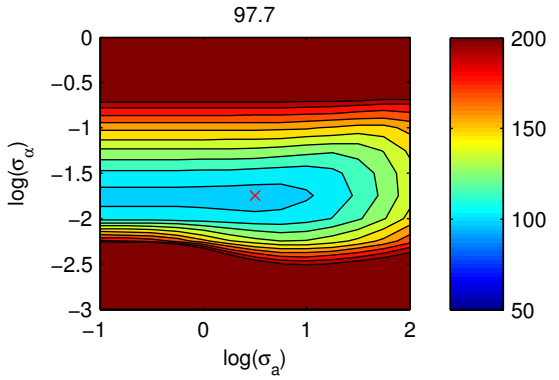

Fig. 4. RMSE as function of noise standard deviation $\log(\sigma_a)$ and $\log(\sigma_\alpha)$ for EKF2 with Cartesian CT model on Trajectory 1. Only segments in which the target maneuvers are taken into account.

Trajectory 5 on which the performance is equally bad. A closer look at Trajectory 5 reveals that it contains both segments of very little maneuvering (constant low acceleration) and heavy maneuvering and is as such difficult to handle with a single filter. Changing from Cartesian EKF to EKF2 does not yield significantly different performance but has another interesting effect. The obtained RMSE values become less sensitive to variations in σ_a. This can be seen by comparing Figures 4 and 5 that were obtained with the same model. A similar observation has been made in [6] where EKF2 is said to improve robustness of a Cartesian velocity CT EKF. Apart from this desirable effect, EKF2 significantly increases the computation time. Owing to the sparsity of the required Hessian matrices; however, the computations could be significantly reduced by utilizing the problem structure.

A comparison of Cartesian UKF variants yields the results of Figure 6 which are comparable to the EKF in Figure 5 on Trajectories 3–6 and slightly worse on Trajectories 1 and 2. Again, $G_c^2(h)$ of (7a) gives the best results, but also using the simple G_c^3 of (7b) performs well. Similar to EKF2, the UKF seems to be less sensitive to changes in σ_a than the EKF.

We next turn to the CT models with polar velocity. The matrices G_p^1 and $G_p^2(h)$ in (5) give rise to two variants. For

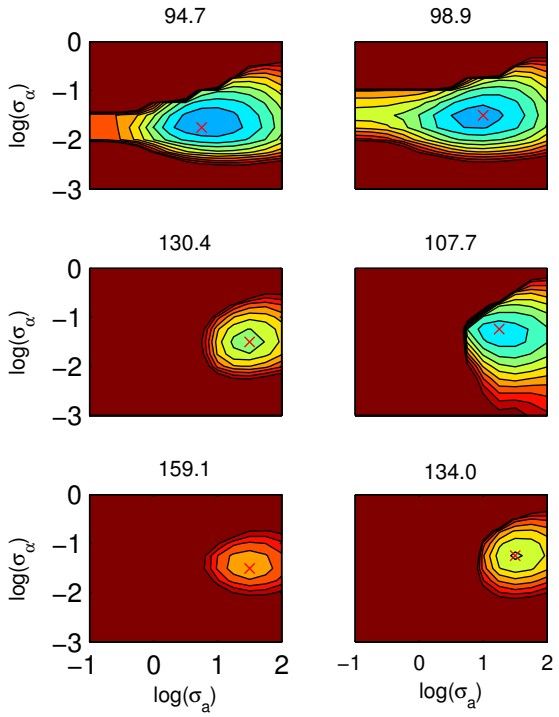

Fig. 5. RMSE on all trajectories for the best EKF with Cartesian CT model. Color bar given in Figure 4. Arrangement of trajectories similar to Figure 2.

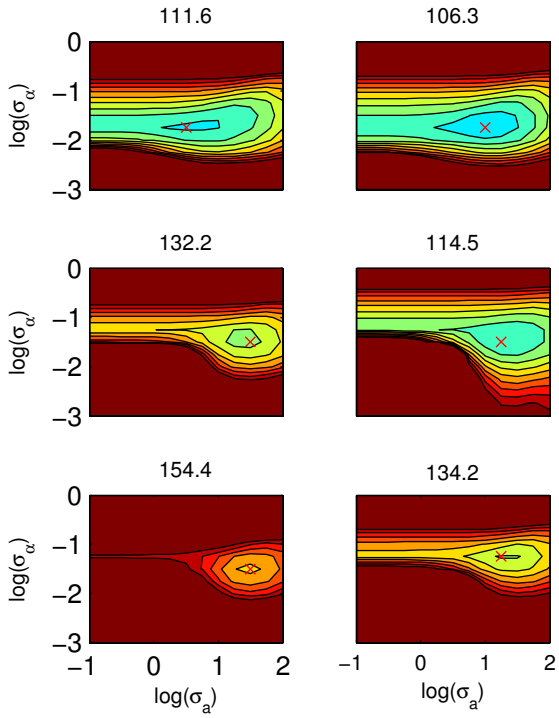

Fig. 6. RMSE on all trajectories for the best UKF with Cartesian CT model. Color bar given in Figure 4. Arrangement of trajectories similar to Figure 2.

EKF, the results show little preference for either of the two, so we present the results for $G_p^2(h)$ in Figure 7. These show another improvement over the EKF with Cartesian CT model. The regions of low RMSE on Trajectories 1 and 2 appear larger than for all Cartesian CT filters. The filter is robust to deviations from the optimal σ_a and σ_α.

Changing to EKF2 does not yield any significant improvements which might be explained by the fact that the lower part of (4) is actually linear. The corresponding Hessian matrices are zero. A similar statement can be made for UKF, as shown in Figure 8 for $G_p^2(h)$.

C. Summary

We made the following observations. For the considered trajectory segments, the use of nonlinear Kalman filters with coordinated turn models yields an improvement over a linear Kalman filter with constant velocity model.

For Cartesian velocity UKF and EKF2 can reduce the sensitivity to the process noise parameters. Still EKF shows the best quantitative performance. In terms of the model, a state dependent input matrix $G_c^2(h)$ from (7a) appears best if a Cartesian velocity representation is used.

Using polar velocity representation instead can yield a further decrease in RMSE. Here, the choice of input matrix (5) is less significant. UKF and EKF provide comparable accuracy.

The RMSE contour plots in Figures 4 to 8 reveal that each individual algorithm can be run with the same parameter settings for all trajectories without much increase in RMSE. The optimal σ_α are close for all trajectories, the optimal σ_a are close for Trajectories 3 to 6, and the RMSE is less sensitive to σ_a for Trajectories 1 and 2 (i.e., for the least agile targets).

V. Concluding Remarks

We have shown a range of coordinated turn (CT) models using either Cartesian or polar velocity and how to use them in a Kalman filtering framework for maneuvering target tracking. The results of the conducted simulation study are in favor of polar velocity. This confirms the results of the previous study [11] and extends it to the case of varying target speed. For polar CT models, the performance in terms of position RMSE of the predicted state appears to be comparable for EKF and UKF. As the UKF does not require the derivation and implementation of Jacobians it might be more straightforward to implement. The RMSE provided by the Cartesian velocity EKF and UKF turned out slightly worse. Interestingly, the sensitivity of the RMSE with respect to the noise parameters was decreased by using EKF2 and UKF in the Cartesian case. This, in addition to the simpler implementation and lower computational cost of UKF over EKF2 results in a recommendation for UKF if Cartesian CT models are preferred.

Our results indicate that for each CT filter there is one set of noise parameters that yields good performance on all investigated trajectories, although the maneuver characteristics are quite different from trajectory to trajectory. Furthermore, we have shown that the use of such flexible CT filters yields improved results (on maneuvering targets) when compared to a well tuned linear KF with constant velocity model. These

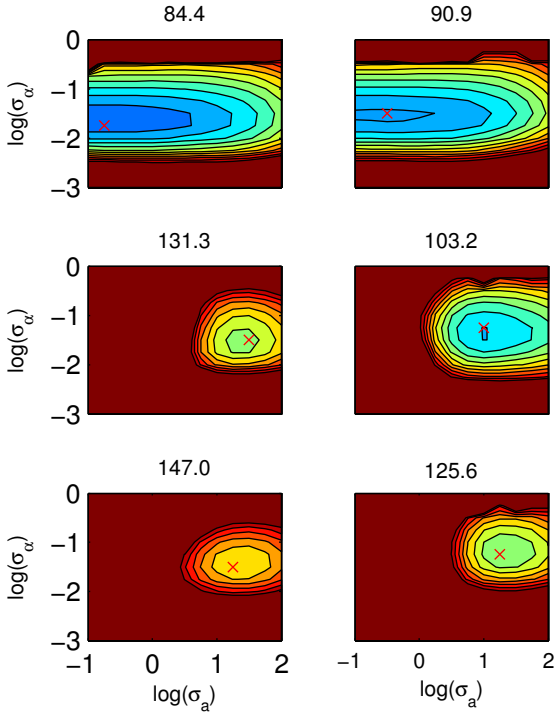

Fig. 7. RMSE on all trajectories for the best EKF with polar CT model. Color bar given in Figure 4. Arrangement of trajectories similar to Figure 2.

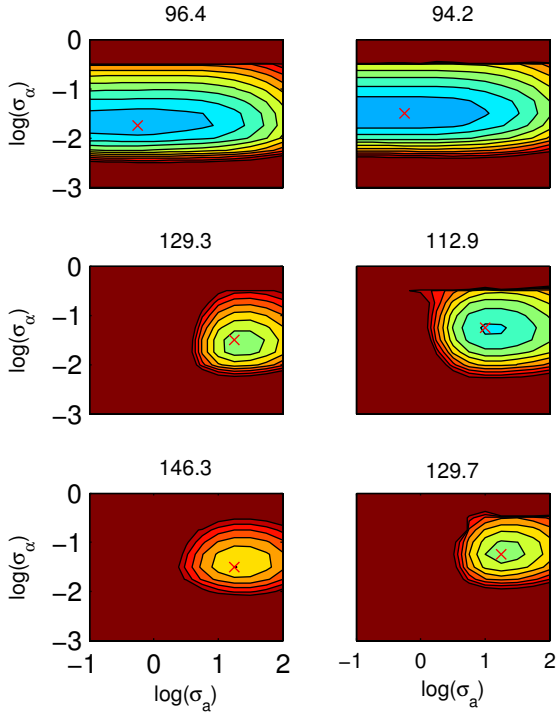

Fig. 8. RMSE on all trajectories for the best UKF with polar CT model. Color bar given in Figure 4. Arrangement of trajectories similar to Figure 2.

insights advocate very much for the use of the investigated CT filters in IMM tracking algorithms.

Acknowledgment

The work was supported by the project Cooperative Localization (CoopLoc) funded by Swedish Foundation for Strategic Research (SSF) and the Swedish strategic research center Security Link.

References

[1] S. Blackman and R. Popoli, *Design and Analysis of Modern Tracking Systems*. Artech House, Aug. 1999.

[2] Y. Bar-Shalom, X. R. Li, and T. Kirubarajan, *Estimation with Applications to Tracking and Navigation*. Wiley-Interscience, Jun. 2001.

[3] Y. Bar-Shalom, P. K. Willett, and X. Tian, *Tracking and Data Fusion: A Handbook of Algorithms*. Storrs, CT: YBS Publishing, 2011.

[4] F. Gustafsson, *Statistical Sensor Fusion*. Studentlitteratur AB, Mar. 2010.

[5] X. R. Li and V. Jilkov, "Survey of maneuvering target tracking. Part I. Dynamic models," *IEEE Trans. Aerosp. Electron. Syst.*, vol. 39, no. 4, pp. 1333 – 1364, Oct. 2003.

[6] P. Vacher, I. Barret, and M. Gauvrit, "Design on a tracking algorithm for an advanced ATC system," in *Multitarget-Multisensor Tracking: Applications and Advances*. Norwood, MA: Artech House, 1992, vol. 2, pp. 1–28.

[7] N. Nabaa and R. Bishop, "Validation and comparison of coordinated turn aircraft maneuver models," *IEEE Trans. Aerosp. Electron. Syst.*, vol. 36, no. 1, pp. 250–259, 2000.

[8] B. D. Anderson and J. B. Moore, *Optimal Filtering*. Prentice Hall, Jun. 1979.

[9] S. J. Julier and J. K. Uhlmann, "Unscented filtering and nonlinear estimation," *Proc. IEEE*, vol. 92, no. 3, pp. 401– 422, Mar. 2004.

[10] M. Mallick, M. Morelande, L. Mihaylova, S. Arulampalam, and Y. Yan, "Comparison of angle-only filtering algorithms in 3D using Cartesian and modified spherical coordinates," in *2012 15th International Conference on Information Fusion (FUSION)*, Jul. 2012, pp. 1392 – 1399.

[11] F. Gustafsson and A. Isaksson, "Best choice of coordinate system for tracking coordinated turns," in *Proceedings of the 35th IEEE Conference on Decision and Control, 1996*, vol. 3, Dec. 1996, pp. 3145 –3150.

[12] W. Blair, G. Watson, T. Kirubarajan, and Y. Bar-Shalom, "Benchmark for radar allocation and tracking in ECM," *IEEE Trans. Aerosp. Electron. Syst.*, vol. 34, no. 4, pp. 1097–1114, Oct. 1998.

[13] M. Morelande and N. Gordon, "Target tracking through a coordinated turn," in *IEEE International Conference on Acoustics, Speech, and Signal Processing, 2005. Proceedings. (ICASSP '05)*, 2005, pp. iv/21–iv/24.

[14] P.-A. Kountouriotis and S. Maskell, "Maneuvering target tracking using an unbiased nearly constant heading

model," in *2012 15th International Conference on Information Fusion (FUSION)*, Jul. 2012, pp. 2249–2255.
[15] J. L. Gertz, "Multisensor surveillance for improved aircraft tracking," *MIT Lincoln Laboratory Journal*, vol. 2, no. 3, pp. 381–396, 1989.
[16] A. H. Jazwinski, *Stochastic Processes and Filtering Theory*. Academic Press, Mar. 1970.
[17] M. Grewal and A. Andrews, "Applications of Kalman filtering in aerospace 1960 to the present," *IEEE Control Syst. Mag.*, vol. 30, no. 3, pp. 69–78, 2010.
[18] M. Nørgaard, N. K. Poulsen, and O. Ravn, "New developments in state estimation for nonlinear systems," *Automatica*, vol. 36, no. 11, pp. 1627–1638, Nov. 2000.
[19] M. Roth and F. Gustafsson, "An efficient implementation of the second order extended Kalman filter," in *Proceedings of the 14th International Conference on Information Fusion (FUSION)*, Jul. 2011.
[20] M. Roth, "Kalman filters for nonlinear systems and heavy-tailed noise," Licentiate thesis, Linköping University, Linköping, Sweden, Sep. 2013. [Online]. Available: http://urn.kb.se/resolve?urn=urn:nbn:se:liu:diva-97544
[21] I. Arasaratnam and S. Haykin, "Cubature Kalman filters," *IEEE Trans. Autom. Control*, vol. 54, no. 6, pp. 1254–1269, Jun. 2009.
[22] F. Gustafsson and G. Hendeby, "Some relations between Extended and unscented Kalman filters," *IEEE Trans. Signal Process.*, vol. 60, no. 2, pp. 545 –555, Feb. 2012.